Received: 7 October 2019 | Revised: 16 December 2019 | Accepted: 22 January 2020

DOI: 10.1002/app.49069

ARTICLE

Applied Polymer SCIENCE WILEY

Evaluation of UV-induced embrittlement of PE-HD by Charpy impact test

Maren Erdmann[1,2] | **Ute Niebergall**[2] | **Volker Wachtendorf**[1] | **Martin Böhning**[1]

[1]Division 7.5, Bundesanstalt für Materialforschung und -prüfung (BAM), Berlin, Germany

[2]Division 5.3, Bundesanstalt für Materialforschung und -prüfung (BAM), Berlin, Germany

Correspondence
Martin Böhning, Bundesanstalt für Materialforschung und -prüfung (BAM), Unter den Eichen 87, 12205 Berlin, Germany.
Email: martin.boehning@bam.de

Funding information
Bundesanstalt für Materialforschung und -Prüfung

Abstract

The impact fracture behavior of two common high-density polyethylene grades for container applications were intensively studied by the instrumented Charpy impact test after well-defined exposure to UV-irradiation. Individual stages of the impact event, such as crack initiation and crack propagation energy as well as maximum impact load, were investigated from the recorded load–deflection curves. UV-induced material property changes were further investigated by infrared spectroscopy, differential scanning calorimetry, and dynamic-mechanical analysis as well as density measurements. Based on the results of the Charpy impact test, three indicators were identified to describe the extend of photooxidation on high-density polyethylene: (a) a reduced Charpy impact strength—at least to half of its initial value for a distinctly brittle impact fracture, (b) a marked decrease in the crack propagation contribution to the impact strength, and (c) an increase of the brittle features of the fracture surface.

KEYWORDS

degradation, mechanical properties, packaging, polyolefins

1 | INTRODUCTION

High-density polyethylene (PE-HD) is one of the most widely applied semicrystalline material for packaging application as it is resistant to environmental stress cracking, chemical attack and mechanical impact and provides good processability.[1] As packaging material for storage of chemicals and hazardous goods, PE-HD must withstand the exposure to environmental factors without its functionality being affected.

However, solar irradiation on polyethylene in outdoor applications over years can lead to deterioration of material properties.[2,3] Theoretically, polyolefins should be transparent to ultraviolet (UV) radiation, but the presence of impurities enables the absorption of UV radiation which can cause photodegradation.[4,5] In the presence of oxygen this photooxidation, following the autooxidation mechanism from Bolland and Gee, proceeds in three stages: initiation, propagation, and termination.[6] This UV-induced degradation preferably occurs in the amorphous regions rather than in the more dense and rigid crystalline phase and can result in chain scission and/or crosslinking.[5,7,8]

Photooxidation predominantly occurs very rapidly near the polymer surface while the reaction rate in the inner bulk is low because of a limited amount of oxygen

available inside (diffusion limited oxidation [DLO]) resulting in an U-shaped distribution of oxidation products over the depth of the sample.[8–10] In order to avoid difficulties related to DLO effects, degradation studies are often performed on thin films.[2,11,12] Degradation and the deterioration of the macroscopic material properties can be revealed by discoloration,[4] melting behavior changes,[11] or reduced mechanical strength and elongation at break.[7,11,13–15] Especially, semicrystalline polymers show an abrupt ductile-brittle transition when they undergo aging by random chain scission.[11,13,16]

Only few studies are addressing the progress of degradation on bulk specimens by alternative methods such as microhardness[17] or impact fracture test.[14] The Charpy impact test is a widely applied standard method to evaluate fracture toughness of polymers, for example, for polymeric storage tank applications. It is advantageous as a cost-effective material testing procedure not only for quality control but also for the characterization of polymer blends[18] and fiber reinforced plastics.[19–21]

While the conventional Charpy impact test provides only an integral value of the consumed energy for the crack,[19,22] the instrumentation of the Charpy test allows a more detailed analysis of the fracture process.[19] From the recorded load–time or load–deflection curve, the integral fracture energy can be separated into contributions for crack initiation and crack propagation. It was shown by Böhning et al that the instrumented Charpy impact test is also sensitive to minor changes of high-density polyethylene induced by fuel sorption.[23,24] Several studies also demonstrated a temperature-dependent Charpy impact strength for thermoplastics.[24,25]

The present article examines two PE-HD materials under prolonged UV-irradiation representing the practical application of a polymeric storage tank exposed to a solar environment for several years. Structural changes of the polymers induced by UV-exposure were investigated by the instrumented Charpy impact test and fracture surface analysis. For further evaluation of the photooxidative material degradation, Fourier-transform infrared spectroscopy/attenuated total reflection (FT-IR/ATR), oxidative induction time (OIT), differential scanning calorimetry (DSC), and dynamic-mechanical analysis (DMA) are performed and correlated with the determined Charpy impact behavior.

2 | MATERIALS AND METHODS

2.1 | Material

Two different grades of high-density polyethylene were selected for this research. Both polymers were supplied by LyondellBasell (Frankfurt/M., Germany) as granules and are typically used for container applications, including those for the transport of dangerous goods. The two polyethylene grades examined are designated as PE-HD 1 and PE-HD 2[26] and their characteristic properties are compiled in Table 1.

TABLE 1 Compilation of properties for both investigated PE-HD

	PE-HD 1	PE-HD 2
Density ρ (g/cm^3)	0.949	0.960
Melt flow rate[a] (190°C, 21.6 kg) (g/(10 min))	6	23
Melting peak temperature $T_{p,m}$ (DSC) (°C)	135	141
Crystallinity X_c (DSC) (%)	70	79
OIT[b] at 180°C (min)	436	74
Notched Charpy impact strength a_{cN} at −30°C instrumented determined (kJ/m^2)	16	19
Yield stress[b] σ_y (MPa)	25	32
Yield strain[b] ε_y (%)	11	9

Abbreviations: DSC, differential scanning calorimetry; OIT, oxidative induction time; PE-HD, high-density polyethylene.
[a]From technical data sheet.
[b]From Reference [26].

However, PE-HD 1 presents a lower density ρ, crystallinity X_c, and melting peak temperature $T_{p,m}$ compared to PE-HD 2. As to the differences in the mechanical values, PE-HD 1 has also slightly lower notched Charpy impact strength a_{cN}, yield stress σ_y, and higher yield strain ε_y. The OIT in the polymer melt at 180°C is higher by a factor of 6 for PE-HD 1 compared to PE-HD 2. PE-HD 1 can be processed by extrusion thermoforming and extrusion blow molding. On the other hand, the significantly higher melt flow rate (MFR = 23 g/(10 min)) for PE-HD 2 indicates that it is also processable by injection molding.

2.2 | Sample preparation

Sheets of thicknesses $h = 4$ mm and $h = 1$ mm were obtained by compression molding and the preparation was performed according to the standard procedure following ISO 293[27] as reported earlier.[23,24,28,29] After melting of the polymer granules at a temperature of 180°C for 5 min in the heating press, a pressure of 10 MPa was applied. The sheets were then cooled with a rate of 15 K/min and subsequently annealed at 100°C for 3 hr.

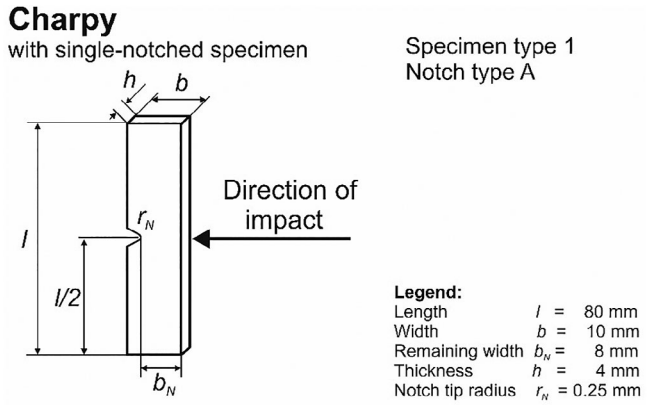

FIGURE 1 Scheme of a notched specimen for the Charpy impact test, type 1A according to Reference [22]

Charpy specimens of the geometry shown in Figure 1 were machined from the 4 mm plates. The specimen dimensions present a thickness $h = 4$ mm, a width $b = 10$ mm, and a length $l = 80$ mm. The notch with a depth of 2 mm was machined into the specimen center located at $l/2$. Thus, the remaining width b_N at notch tip was 8.0 ± 0.2 mm and the radius of the notch tip was $r_N = (0.25 \pm 0.05)$ mm (type A) (see Figure 1). The direction of impact during the Charpy impact test was edgewise on the specimen (method designation ISO 179-1/1eA[22]). It should be noted that the notches were machined into the Charpy specimens before UV-irradiation as described in the following section.

2.3 | UV exposure conditions

The notched specimens for Charpy impact test and sheets with thickness of 1 mm were exposed in an artificial weathering device Global UV Test 200 from Weiss-Umwelttechnik (Reiskirchen, Germany). It was equipped with UV-A 340 nm fluorescent lamps of type 1A according to ISO 4892-3 that show good correlation to the actinic part of the spectral distribution of solar global radiation. Since the lamps have hardly any visible or IR contribution, the emission's radiation heating of the samples was within 1 K.[30] The lamps were mounted vertically in the door of the weathering device.

Samples were positioned vertically in parallel to the UV-irradiation lamps standing upright on stainless steel racks in the presence of circulating air. They were mounted using small stripes of adhesive tapes on their backs and UV-irradiation was applied from one side only. This experimental setup is designed to match the possible outdoor sunlight irradiation of PE-HD transport containers. Thus, the side facing the UV-lamps were much more exposed to radiation than the backside resulting in an asymmetric U-shaped distribution of oxidation products. A temperature of 60°C was chosen to moderately accelerate the degradation process. Such a temperature is reasonable as from experience under typical outdoor conditions with global irradiation (noon-maximum, no clouds, typical convection, 30–40°C ambient temperature) a container made from an uncolored PE-HD material would at least reach a maximum of 50°C due to radiation heating.[31]

The resulting atmosphere was dry, below 15 %RH. The combination of exposure factors, for example, UV and temperature, shows a synergistic effect leading to a more severe damage than both exposure factors being applied separately and sequentially. The natural UV-radiance exposure of the longest artificial UV-irradiation in this study (500 MJ/m^2 achieved after 4,200 hr) was approximately equivalent to 2 years in southern Florida, with an annual solar radiant exposure of 280 MJ/m^2[32] (in terms of the pure UV equivalent, not considering the higher temperature in the artificial test).

The UV-irradiance for the artificial exposure was 33 W/m^2. The UV-radiative exposure energies H in MJ/m^2 were calculated according to Equation (1).

$$\text{UV}-\text{irradiative exposure energy } H = \frac{\text{irradiance (W/m}^2) \times \text{hours (h)} \times 3{,}600\,\text{(s)}}{1{,}000{,}000} \quad (1)$$

The resulting UV-irradiative exposure energies H for notched Charpy specimens are: 38, 74, 110, 145, 217, 278, 357, and 500 MJ/m^2, respectively. The UV-exposure energies H for the 1 mm sheets are: 110, 217, 330, and 460 MJ/m^2.

For comparison control samples for both PE-HD were subjected to a purely thermal treatment (oven storage) at 60°C for more than 2 years.

2.4 | Instrumented Charpy impact test

The instrumented Charpy impact tests were performed according to ISO 179-2.[33] The pendulum impact testing machine Zwick B5113E (Ulm, Germany) was equipped with a semiconductor strip at the 4 J pendulum hammer, a Wheatstone bridge and a signal amplifier that detects the load for the impact fracture. The signal was recorded using a digital storage oscilloscope Hameg 1507-3 operated via a RS-232 interface by the WinIKBV software, version 1.0, of PSM (Polymer Service GmbH, Merseburg, Germany). The same Charpy impact equipment was used in a previous publication[24] and is similar to the one described by Hristov et al.[19] The obtained load–time

(F–t) diagrams or load–deflection (F–s) diagrams from the recorded data were further analyzed; deflection was calculated from the time-dependent signal by the software WinIKBV.

Specimens were cooled down to a testing temperature of −30°C in a temperature-controlled chamber using liquid nitrogen as cooling medium. In total, six specimens were tested for each UV-irradiation exposure energy. An arithmetic mean and a coefficient of variation were determined for each test series.

In general, the Charpy impact strength a_{cN} is expressed by the absorbed impact energy at break W_b and the initial cross-sectional area of the specimen (Equation (2)):

$$a_{cN} = \frac{W_b}{h \times b_N} \times 10^3 \quad (2)$$

The cross-sectional area is defined by the sample thickness h and the remaining width b_N excluding the notch of 2 mm (see Figure 1).

The recorded fracture process (load–deflection curve) in Figure 2a can be evaluated with respect to the crack initiation energy W_i up to the maximum impact load F_m and the following crack propagation energy W_p.[34] Thus, the total energy until break W_b is composed of the sum of crack initiation energy W_i and crack propagation energy W_p (Equation (3)) and was analyzed by the software WinIKBV. All shown load–deflection diagrams are unmodified curves as obtained from the instrumentation of the Charpy impact test.

$$W_b = W_i + W_p \quad (3)$$

The fracture scheme in Figure 2b illustrates that the impact of the pendulum hammer is located on the opposite side of the notch. The crack opens at the notch and the direction of crack growth is reverse to the impact. On the resulting fracture surfaces of the notched Charpy impact specimen up to seven characteristic zones can be distinguished, as shown schematically in Figure 2c and based on the References [24, 34]. Adjacent to the notch (1) (bottom) the fracture mirror is located (2) which is attributed to crack initiation and stable crack growth.[24] The subsequent brittle zone (3) is characteristic for fast and unstable crack propagation. Furthermore, an area with alternating ductile and brittle fracture (4) can occur, followed by a ductile zone (6). The formation of a pronounced white compression zone (7) is characteristic for a soft and ductile impact behavior. If the hinge is present (8), this is located opposite to the notch. White shear lips (5) can occur on the outer areas of the fracture surface. Fracture surface analysis of the characteristic fracture zones was conducted on a stereo microscope Stemi 2000C from Carl Zeiss AG (Oberkochen, Germany) equipped with an AxioCam ICc 3 and AxioVs40x64V 4.9.1.0 software.

2.5 | FT-IR/ATR

The degradation progress on the surface of the Charpy bulk specimens was investigated by FT-IR in ATR mode. Measurements were performed on a FT-IR spectrometer Nicolet 6700 with a diamond ATR crystal and a DTGS KBr detector. The extinction spectra were recorded by the OMNIC software (Version 9). The recorded spectra

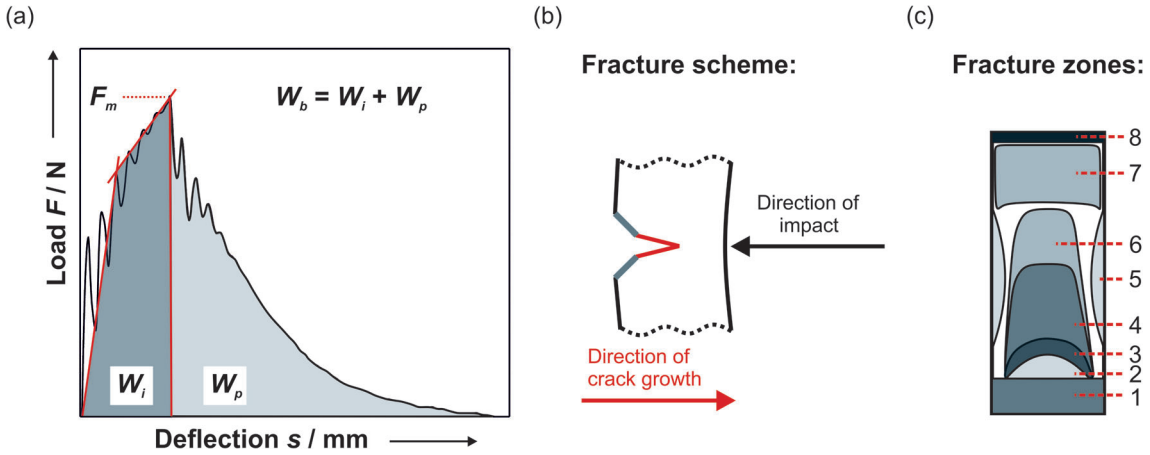

FIGURE 2 Schematic load F–deflection s curve indicating crack initiation W_i, crack propagation energy W_p, and maximum impact load F_m (a), fracture scheme of the crack opening for a notched specimen in the Charpy impact test (b), and scheme of designated fracture zones (c) [Color figure can be viewed at wileyonlinelibrary.com]

averaged 32 scans at a resolution of 4 cm^{-1}. The wavenumber range was from 4,000 to 400 cm^{-1} and background spectrum was refreshed every 15 min. The supplied standard ATR correction from the OMNIC software was used.

FT-IR/ATR spectra were collected on three different positions on the UV-exposed surface. This was performed on two specimens each for defined UV-irradiation exposure energy H. For visualization of the spectra, they were averaged with a tool provided from the OMNIC software. The averaged spectra were normalized to the respective peak height of the internal reference band at 2,912 cm^{-1}, assigned to the $-CH_2-$ groups, due to their sufficiently stable nature.[20] The carbonyl index (CI) was calculated by the ratio of the integrated area of carbonyl absorption band (1,816–1,600 cm^{-1}) to the reference band (2,977 and 2,865 cm^{-1}).

2.6 | Differential scanning calorimetry

DSC experiments were performed using a DSC 204 F1 Phoenix and the software Proteus–Thermal Analysis Version 6.1.0 from NETZSCH-Gerätebau GmbH (Selb, Germany). The temperature range of the measurements was from −50 to 180°C at a rate of 10 K/min (heating and cooling) and a nitrogen flow rate of 250 ml/min. Samples with a mass of 10–13 mg were punched from the UV-exposed 1 mm sheets. DSC analysis and determination of melting enthalpy and temperature were performed according to Reference [35]. The heat of melting ΔH_m was determined in a fixed temperature range (50–170°C, tangential baseline). The temperature at maximum heat flow presents the melting peak temperature $T_{p,m}$. The degree of crystallinity X_c was calculated according to Equation (4) and applying the theoretical heat of melting $\Delta H_m^{100\%} = 293\,J/g$ for 100% crystalline polyethylene.[29]

$$X_c = \frac{\Delta H_m}{\Delta H_m^{100\%}} \times 100\,[\%] \tag{4}$$

The number of samples for a distinct UV-irradiation was $n = 3$ to calculate the arithmetic mean and error.

2.7 | Oxidation induction time

The OIT, specified, for example, in ISO 11357-6,[36] is a relative measure of resistance against oxidative decomposition of a material reflecting predominantly the stabilization against oxidation by respective additives. For this method, a DSC 204 F1 Phoenix from Netzsch-Gerätebau GmbH (Selb, Germany) was used, equipped with the software Proteus–Thermal Analysis, Version 6.1.0.

Heating was performed from room temperature to 180°C at 10 K/min in nitrogen atmosphere, the isothermal stabilization time at 180°C was 5 min, followed by an oxygen flushing with 250 ml/min under isothermal conditions. The isothermal OIT was determined from the obtained heat flow curve by the intercept of tangent method. The polymer specimens, having masses between 4.3 and 6 mg, were cut from the compression molded sheets of 1 mm thickness. OIT measurements were carried out for the reference state as well as after 217 and 460 MJ/m^2 UV-irradiation. The measurements were performed at least in triplicate for each polyethylene sample.

2.8 | Density measurements

Densities were determined for unexposed and UV-irradiated PE-HD based on the Archimedes principle using an analytical balance MC 410 S Sartorius (Göttingen, Germany) with density determination kit. The polymer samples were weighed in air (m_{air}, $\rho_{air} = 0.0012\,g/cm^3$) and subsequently in liquid n-heptane ($m_{n-heptane}$, $\rho_{n-heptane} = 0.684\,g/cm^3$). Equation (5) was applied for the density calculation of PE-HD.

$$\rho = \frac{m_{air}}{m_{air} - m_{n-heptane}} \left(\rho_{n-heptane} - \rho_{air}\right) + \rho_{air} \tag{5}$$

Disk-shaped samples with a diameter of 10 mm and a thickness h of about 1 mm were punched out of the plane sheets. The density measurements were performed for $n = 4$ samples and for H of 0, 110, 217, 330, and 460 MJ/m^2.

2.9 | Dynamic-mechanical analysis

The dynamical mechanical analysis was performed on a DMA/SDTA 861e (Mettler-Toldeo, Greifensee, Switzerland) and STARe-software Version 15. The shear mode was chosen because it allows to investigate the course of the shear storage G' and loss modulus G'' from the low temperature region up to the polymer melt. The specimen had a rectangular geometry with length l and width b of about 10 mm and a thickness h of about 1 mm (further information is found in Figure S1). Heating scans were performed in the temperature range between 25 and 200°C at 3 K/min and at a frequency f of 10 Hz. The maximum displacement (amplitude) was 3 μm and the maximum force of 10 N. All measurements were performed at least in duplicate.

3 | RESULTS AND DISCUSSION

3.1 | Instrumented Charpy impact test

The following impact parameters, such as Charpy impact strength a^*_{cN} (Figure 3), crack initiation energy W^*_i, crack propagation energy W^*_p, and maximum impact load F^*_m (Figure 5) were determined at −30°C and are presented normalized relative to their respective original reference value (see Table S1). First, the determined normalized Charpy impact strength a^*_{cN} calculated by the integral energy at break W_b for UV-irradiative exposure energies H from 0 to 500 MJ/m^2 on both high-density polyethylene grades are compared in Figure 3.

In case of PE-HD 1, the impact strength shows only slight changes for UV-exposure energies up to 74 MJ/m^2. The a^*_{cN}-values decrease almost to the half of their initial reference value for $H = 110$ MJ/m^2 and $H = 145$ MJ/m^2. For 217 and 278 MJ/m^2 the impact strength is further reduced to 0.4. Continuing UV-exposition keeps a low level of normalized impact strength of $a^*_{cN} = 0.3$ (see Figure 3).

The course of the normalized Charpy impact strength differs significantly for PE-HD 2 (Figure 3). Here, drastically reduced impact values of $a^*_{cN} = 0.2$ are already obtained for the lowest H of 38 MJ/m^2. The normalized Charpy impact strength values remain at this low constant plateau on further irradiation with a^*_{cN} of about 0.3. The course of the normalized Charpy impact values a^*_{cN} in Figure 3 reveals the different sensitivities to UV-irradiation of the two polyethylene grades which is in agreement with the determined oxidation induction times (Section 3.3) indicating a better stabilization of PE-HD 1.

For further analysis of the different impact behavior of both polymers, the obtained fracture surfaces (left) and the corresponding load F–deflection s curves (right) for distinct UV-irradiative exposure energies H are displayed in Figure 4. While the conventional Charpy impact test only provides an integral value of the energy at break W_b, the instrumentation of the fracture process allows to differentiate between crack initiation energy W_i and crack propagation energy W_p (see Figure 2). The constituent partial energies correspond to the respective areas under the curve, which are highlighted in the diagrams.

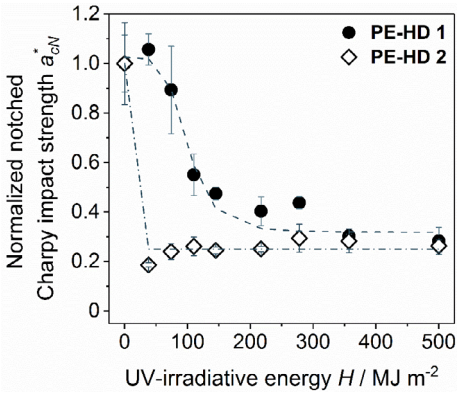

FIGURE 3 Progress of the normalized notched Charpy impact strength a^*_{cN} with increasing UV-radiation exposure energy H from 0 to 500 MJ/m^2 for PE-HD 1 and PE-HD 2 [Color figure can be viewed at wileyonlinelibrary.com]

The fracture surfaces of both unexposed PE-HD's (Figure 4a, 0 MJ/m^2) exhibit well defined characteristic features of brittle (3), ductile (6), and compression zone (7) that can be assigned to a somewhat ductile fracture. The shear lips (5) occur at the outer side of the fracture surface and the hinge (8) opposes the notch (1). A weakly developed alternating ductile/brittle zone (4) can be recognized. The crack arrest lines confining the fracture zones are convex to the notch due to the direction of crack propagation away from the notch. The slightly higher Charpy impact strength for PE-HD 2 ($a_{cN} = 19$ KJ/m^2) compared to PE-HD 1 ($a_{cN} = 16$ KJ/m^2) is consistent with the ductile fracture contributions of zones (4) and (6). With respect to the recorded F-s diagram, both polyethylenes show a pronounced crack initiation energy W_i indicative for elastic and plastic deformation. The crack propagation energy W_p initiated at the load maximum F_m is well developed and more attributable to a ductile fracture. In the following, only the fracture surface zones showing distinct changes are considered.

For PE-HD 1 exposed to $H = 38$ MJ/m^2 in Figure 4b, the fracture surface and the load–deflection curve are nearly unchanged, which also corresponds to the almost constant normalized notched Charpy impact value a^*_{cN} and the ductile fracture behavior. The first distinct changes of the fracture surface zone contributions are observed starting at 74 MJ/m^2 (Figure 4c). Here, the brittle zone (3) becomes more dominant, whereas the contributions of the ductile (6) and the compression zone (7) become smaller. As can be seen from the recorded fracture diagram, the crack initiation energy W_i and load maximum F_m remain constant, whereas the propagation energy W_p decreases noticeably, thus resulting in a lower impact strength a^*_{cN}.

For further UV-irradiation of PE-HD 1 the brittle fracture surface contribution (3) is the most dominating feature (see 145 MJ/m^2 in Figure 4d). The load–deflection curve reveals constant W_i and F_m but the propagation energy W_p diminishes, so that the resulting impact value is reduced to $a^*_{cN} = 0.48$. The crack energy contributions for $H > 145$ MJ/m^2 (PE-HD 1) are no longer distinguishable in the F–s diagram and the corresponding area is

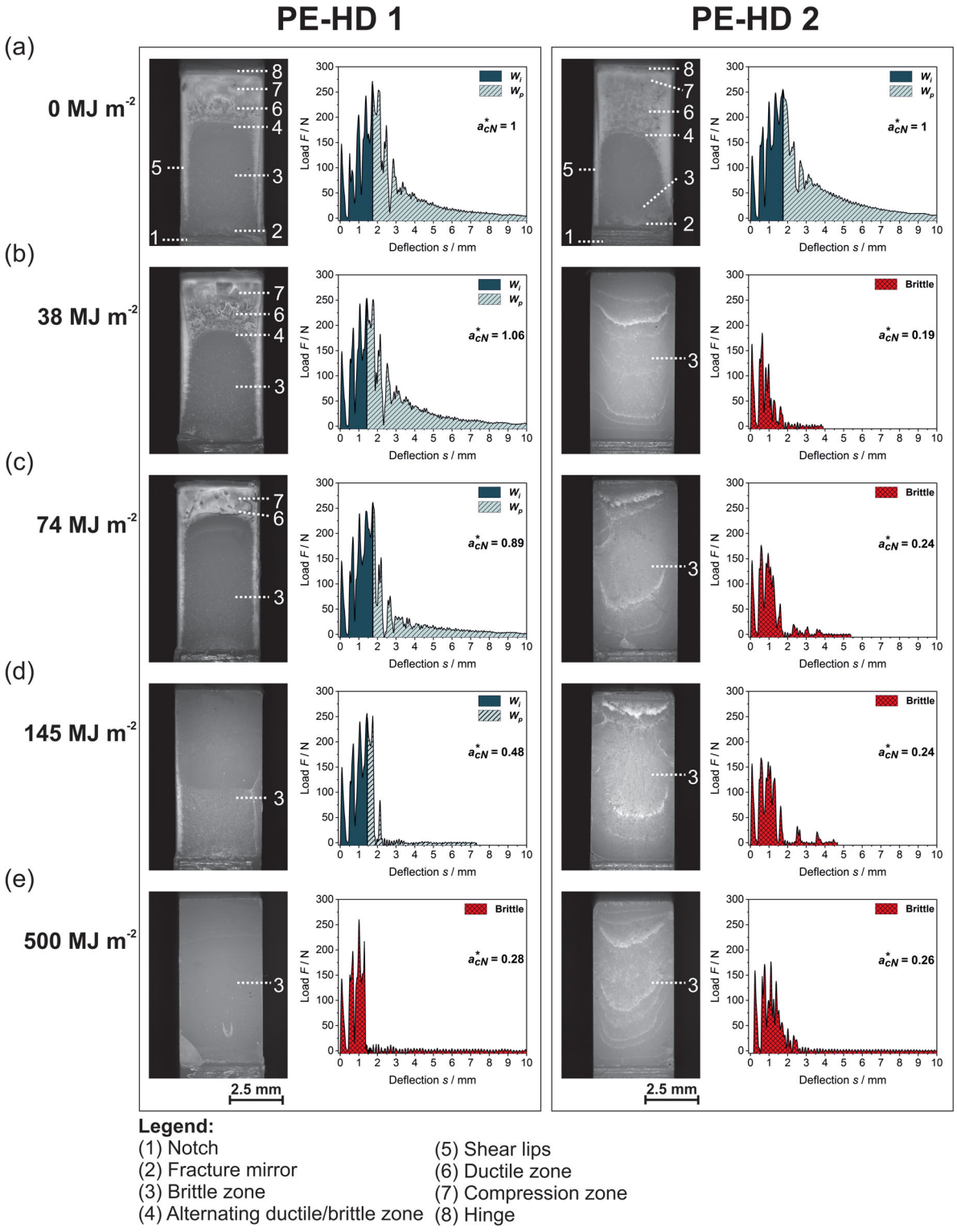

FIGURE 4 Representation of the fracture surfaces and load F—deflection s curves obtained from the instrumentation of the Charpy impact test showing PE-HD 1 (left) and PE-HD 2 (right) for UV-irradiative exposure energies H of 0 MJ/m^2 (a), 38 MJ/m^2 (b), 74 MJ/m^2 (c), 145 MJ/m^2 (d), and 500 MJ/m^2 (e); notch is located at the bottom of the image; Charpy impact test was conducted at a temperature of −30°C [Color figure can be viewed at wileyonlinelibrary.com]

highlighted in red to indicate this brittle fracture. In addition, the fracture surface in Figure 4e is completely smooth (3) with only slightly visible crack arrest lines (PE-HD 1, 500 MJ/m^2). The normalized notched Charpy impact value of $a^*_{cN} = 0.28$ is significantly lower than the half of the initial value.

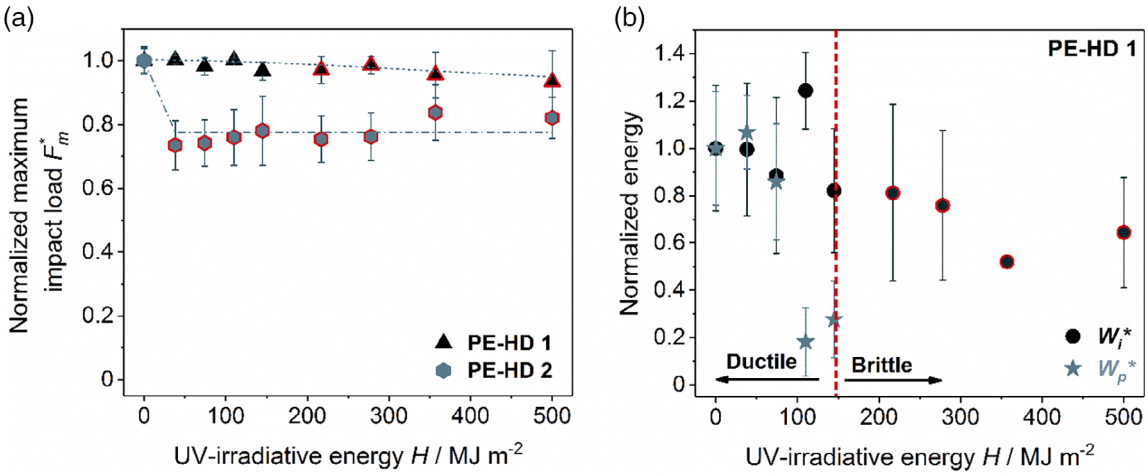

FIGURE 5 Progress of the normalized maximum impact load F_m^* of PE-HD 1 and PE-HD "2 (a) and normalized energy of crack initiation W_i and crack propagation W_p of PE-HD 1 (b); red-bordered symbols designate "brittle" fracture ($a_{cN}^* \leq 0.5$) and the red dashed line indicates the ductile-brittle transition for PE-HD 1; errors represent the standard deviation obtained from six specimens [Color figure can be viewed at wileyonlinelibrary.com]

In case of the photooxidized PE-HD 2, flat brittle zones (3) are observed on all fracture surfaces from the lowest (38 MJ/m^2) to the highest UV-irradiation exposure energy (500 MJ/m^2) as depicted in Figure 4b–e, right. Also, a distinction between the crack energy constituents W_i and W_p from the recorded load–deflection curves cannot be made, not even for the lowest UV-irradiation energy (38 MJ/m^2) (see Figure 4b). This brittle fracture is indicated by the red area in the respective load–deflection diagram. The corresponding crack propagation energies are practically zero. Moreover, the rising tangent in the initial stages of the load–deflection curve is also absent, which in contrast is present in all curves of PE-HD 1 and the reference state of PE-HD 2.

Furthermore, it needs to be highlighted here that the crack arrest lines (fracture lines) are inverted for all photooxidized samples of PE-HD 2 (see scheme in Figures 2 and 4b–e, right), that is, they are concave to the notch. The direction of the parabolic crack arrest lines suggests that the crack is growing toward the notch. The severe embrittlement of the material leads to an anomalous crack initiation at the spot of hammer impact and the crack takes the direction of the impact instead of propagating from the opposite notch inwards, as intended in the Charpy test.

Figure 5a summarizes the normalized maximum impact load F_m^* for both polyethylenes determined from the load–deflection curves; the red-bordered symbols designate "brittle" fracture. As to PE-HD 1, the impact load F_m^* shows nearly no effect (only a slight continuous decrease) when the material is exposed to UV-irradiation. On the other hand, for PE-HD 2 the normalized maximum impact load reduces to 0.8 already at the lowest UV irradiation energy and remains at this level after further irradiation. In summary, the present results from the Charpy impact test for PE-HD 2 strongly suggest a rapid deterioration and embrittlement of the material upon irradiation with UV. This can be seen from the immediate reduction of a_{cN}^* to values < 0.5, where a differentiation of the crack energy components is no longer possible, from the lower plateau values of F_m^* and the inverted crack arrest lines at the fracture surface, that is, the reversed crack propagation.

Due to this immediate embrittlement of PE-HD 2 upon UV-irradiation the normalized energy constituents are presented for PE-HD 1 only (Figure 5b). As already evident from the load–deflection diagrams in Figure 4, not only the maximum impact load F_m^* but also the crack initiation energy W_i^* keeps nearly constant within the error-range up to the irradiation level of $H = 145$ MJ/m^2. Thus, the UV-irradiation hardly affects the crack initiation while the propagation energy W_p decreases starting at $H = 74$ MJ/m^2 (see also Figure 4c, d). At UV-exposure energies of 257 MJ/m^2 and higher a complete embrittlement is observed and a differentiation between the partial crack energies is no longer possible. It is well established that photooxidation deteriorates the amorphous regions leading to chain scission and/or crosslinking. Both are causing an embrittlement of the polymer since the amount of the amorphous regions (by crystallization Section 3.4) as well as their molecular mobility allowing for disentanglements are reduced. The ductile-brittle transition for PE-HD 1 in the notched Charpy impact strength is observed for $a_{cN}^* \leq 0.5$ indicated by the red dashed line in Figure 4b.

A control sample for PE-HD 2 was stored in an oven at a temperature of 60°C for more than 2 years. The UV-exposure of 500 MJ/m^2 in the weathering device was achieved after 25 weeks (4,200 hr, ca. 6 months) and is equivalent to about 2 years of outdoor exposure. For the purely thermal treatment the results showed no reduction in the normalized Charpy impact strength a^*_{cN}. As expected, also no significant deterioration was observed under these conditions also for PE-HD 1.

3.2 | FT-IR/ATR spectroscopy

FT-IR spectra were collected at defined UV-exposure energies H for a more detailed analysis of the chemical changes caused by UV-irradiation on both high-density polyethylene grades. The ATR mode was chosen with a penetration depth up to several micrometers representing a qualitative analysis of the characteristic oxidation products at the polymer surface.

The displayed spectra were normalized using the peak height of the (nearly) unchanged reference band at 2,912 cm^{-1}, which is assigned to —CH_2— groups.[20] This allows a comparative evaluation of the absorption band changes. The obtained spectra for both polyethylene grades and increasing H are shown in Figure 6.

Both polymers present a broad absorption band evolving between 3,100 cm^{-1} and 3,660 cm^{-1} exhibiting a maximum at 3,400 cm^{-1} with increasing UV-irradiation. This absorption region is usually ascribed to hydroxyl-groups (OH) but may also be assigned to hydroperoxides (OOH), which appear in the same wavenumber range. They are most probably formed as primary photodegradation products by the UV-irradiation and can be assumed to be quite stable at temperatures below 100°C. The evolution of this hydroxyl/hydroperoxide absorption band is less pronounced for PE-HD 1 compared to PE-HD 2 with increasing UV-exposure.

The most significant changes in the absorption spectra are observed in the carbonyl region between 1,816 and 1,600 cm^{-1} that is attributed the oxidation progress. The characteristic carbonyl groups can be separated into various contributions: ester at 1,737 cm^{-1} (COOR), aldehyde at 1,726 cm^{-1} (C═O) and carboxylic acid at 1,710 cm^{-1} (COOH) and ketone at 1,693 cm^{-1} (C═O). On both polymers, the most intense absorption band is attributed to the aldehyde (1,726 cm^{-1}). The α,β-unsaturated groups, for example, aldehydes and ketones are typical oxidation products of hydroperoxides by forming hydroxyl radicals and alkoxy radicals. The latter can undergo main chain scission (β-cleavage). However, the α,β-unsaturated group is likely to continue to react photochemically by Norrish type I, since carboxylic acid, esters and lactones are found in the spectra as typically formed reaction products. As seen in Figure 6, the carbonyl group already forms at the lowest H of 38 MJ/m^2 but the evolution is more apparent for PE-HD 2 compared to PE-HD 1.

The observed evolution in the absorption region having a peak maximum at 1,176 cm^{-1} may be assigned to the formation of ether groups (COC).[37] The vinyl groups typically found in wavenumber region from 888 to 965 cm^{-1} (vinylidene CH_2═CR_2, vinyl CH_2═CHR, and vinylene CH═CH[38]) are formed in small traces but less pronounced. In summary, the characterisitic degradation products at the surface are more evolved for PE-HD

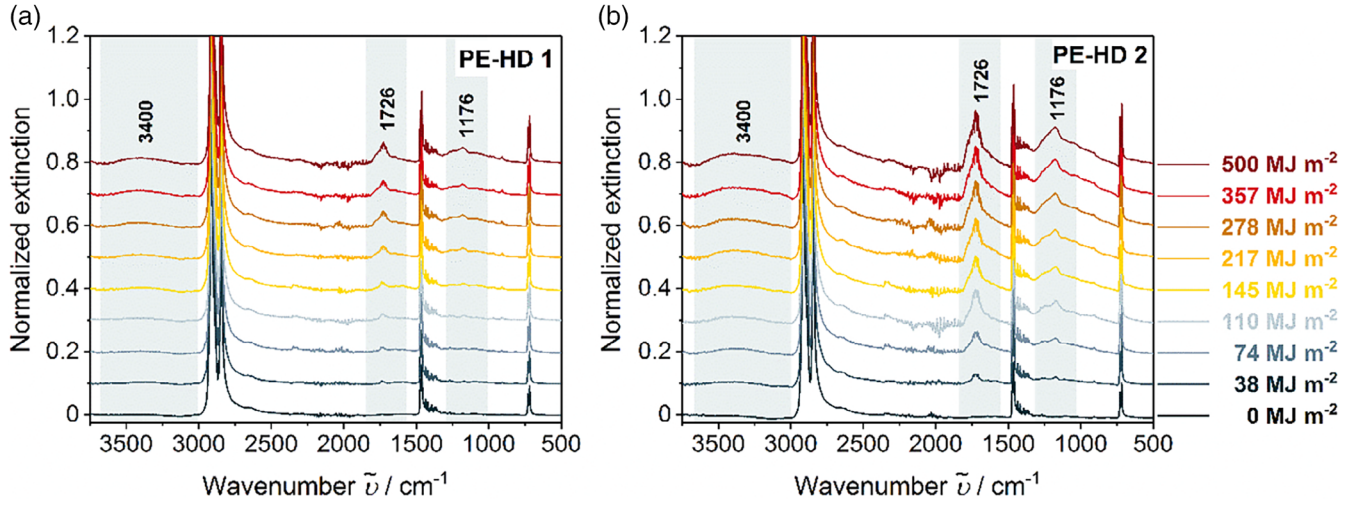

FIGURE 6 Stacked FT-IR/ATR spectra for UV-irradiative exposures energies H from 0 to 500 MJ/m^2 for PE-HD 1 (a) and PE-HD 2 (b); the changing absorption regions as a result of UV-irradiation are highlighted and the corresponding wavenumber absorption peaks are labeled [Color figure can be viewed at wileyonlinelibrary.com]

2 indicating a faster oxidation and material detoriation in agreement with the drastically reduced notched Charpy impact strength (see Figures 3 and 4).

The integrated carbonyl contributions defined as the carbonyl index *CI* for UV-exposure energies *H* from 0 to 500 MJ/m^2 for both polyethylenes are displayed in Figure 7a. As to PE-HD 2, the carbonyl index *CI* shows a rapidly nonlinear raise with increasing UV-irradiation. On the contrary, PE-HD 1 has a rather linear *CI* evolution over UV-irradiation energy *H*. For the highest UV-exposure energy *H* of 500 MJ/m^2 the carbonyl index *CI* of PE-HD 2 is higher by a factor of about three compared to PE-HD 1. Furthermore, the progress of UV-irradiation results in increasing surface roughness and the extinction spectra become noisier, giving rise to an increased error of *CI*, especially noticeable for PE-HD 2.

Figure S4 shows the Charpy impact strength of PE-HD 1 and PE-HD 2 as a function of the respective carbonyl index *CI*.

The hydroxyl/hydroperoxide and carbonyl absorption bands of the control sample for PE-HD 2 after about 2 years thermal treatment are much less pronounced compared to the highest UV-irradiation energy *H* of 500 MJ/m^2 (see Figure S3). Together with the absence of changes in the normalized Charpy impact strength it can be concluded that the UV-irradiation is the dominant factor for the degradation of PE-HD rather than the temperature of 60°C. Thus, the latter is too low within the investigated period of 2 years for inducing appreciable thermal degradation.

3.3 | Oxidation induction time

The following investigations (OIT, DSC, DMA, and density measurements) were carried out on UV-exposed sheet samples with a thickness of $h = 1$ mm. Since the concentration of degradation products decreases with depth due to DLO, these thinner specimens were chosen because the determined bulk properties are more representative for the surface-related degradation.

Changes of the oxidation induction time, regarded as an integral measure for the stabilization by antioxidants, are investigated after selected UV-irradiation exposures as well as for the initial state for both polyethylene grades.

The initial OIT values clearly reveal significant differences in stabilization by antioxidants: PE-HD 1 is distinctly higher stabilized than PE-HD 2 with OIT values of 436 and 74 min, respectively (see Table 1).

The OIT-values for PE-HD 1 when exposed to UV-energy of $H = 217$ MJ/m^2 and $H = 460$ MJ/m^2 are reduced by a factor of 7 to about 64 min in comparison to the neat sample (OIT = 436 min). Although the oxidation induction times for both exposure energies are nearly identical, a higher exothermic heat flow signal is detected for the sample irradiated with 460 MJ/m^2. As to the UV-irradiated PE-HD 2, an intense exothermic heat flow is detected already at the beginning of oxygen introduction. Therefore, the OIT is interpreted as practically zero for PE-HD 2 after exposure to UV-radiation energy of 217 and 460 MJ/m^2.

To summarize, PE-HD 1 still possesses an oxidation resistance and a prolonged stability upon UV-irradiation, while the diminished OIT-value for PE-HD 2 can be interpreted as a complete depletion of stabilizers. Furthermore, these findings for PE-HD 2, indicating a less efficient stabilization, are in agreement with the dramatic loss of ductility in the notched Charpy impact test (Figures 3 and 4) and the pronounced carbonyl evolution (Figure 6). The discussed OIT curves are presented in Figure S2.

3.4 | Differential scanning calorimetry

Crystallinity X_c and peak melting temperature $T_{p,m}$ of unexposed and photooxidized polymers ($H = 460$ MJ/m^2)

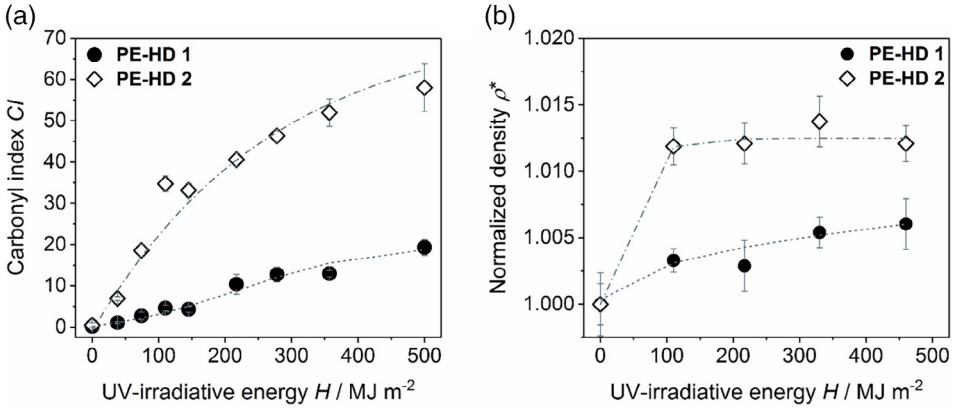

FIGURE 7 Evolution of the MJ/m^2 *CI* (a) and normalized density ρ^* for PE-HD 1 and PE-HD 2 for UV-exposure *H* from 0 to 500 MJ/m^2 (b) [Color figure can be viewed at wileyonlinelibrary.com]

were exemplary determined in DSC on two consecutive heating runs and results are summarized in Table 2. The first melting curve presents the thermal history (initial state of crystallinity), while the second melting characterizes the recrystallization ability of the polymer sample.

The UV-exposure on PE-HD 1 hardly affects its crystallinity and melting peak temperature in the first and in the second melting curve since they remain unchanged in the range of error. As to PE-HD 2, crystallinity and peak temperature in the first heating present significant higher values for the photooxidized polymer ($H = 460$ MJ/m^2). The UV-irradiation probably led to chain scission of, for example, loops and tie chain molecules.[39] The resulting shorter chain fragments have an enhanced mobility which allows incorporation in adjacent crystalline structures. So the material may undergo chemi-crystallization and thus form larger crystals (thicker lamella). Such additional crystallization on irradiated PE-HD is frequently reported.[14,40] As to the second melting for PE-HD 2, crystallinity and peak temperature are drastically reduced. This may be taken as a strong indication for crosslinking induced by formation of radicals due to bond cleavage by UV-irradiation. This leads to intermolecular bond formation resulting in larger macromolecules or network structures.[5] However, it cannot be excluded that the molten polymer and the UV-induced oxidative products mix after the first melting, and these degradation products act as impurities which inhibit crystallization.

3.5 | Density measurements

The normalized densities ρ^* of both PE-HD before and after UV-exposure are displayed in Figure 7b. The density of PE-HD 1 shows a slight increase upon UV-irradiation. For PE-HD 2 a significant density increase is found at the first irradiation level at $H = 110$ MJ/m^2, whereas density remains constant after further exposure. First, the determined density increase may be explained partly by the higher mass of the oxygen (O) incorporated into the polymer chain (—CH_2—CH_2—) compared to the abstracted hydrogen (H).[41,42] Second, the additional UV-induced crystallization as detected by DSC also contributes significantly to the increasing density since the crystalline regions exhibit a higher density than the amorphous phase.[42,43] Especially for PE-HD 2 these density measurements correlate well with the more pronounced carbonyl buildup in Figure 6b (FT-IR/ATR) and the crystallinity X_c from the first melting in DSC (Table 2) and brittle impact fracture in Charpy (Figures 3 and 4).

3.6 | Dynamic-mechanical analysis

The structural changes induced by photooxidation in PE-HD were also examined by DMA in shear mode. The temperature dependency of shear storage modulus G' and shear loss modulus G'' for both unexposed PE-HD are shown in Figure 8a and b. By comparing the courses of the storage moduli in the solid state up to a temperature of 130°C, higher G' values are noticeable for PE-HD 2 attributed to its higher crystallinity and stiffness compared to PE-HD 1. The following drastic decrease of both moduli by about three orders of magnitude is indicative for the beginning of melting. In case of PE-HD 1, the melting occurs at 132°C and for PE-HD 2 at a slightly higher temperature of 138°C, but both polymers present a similar behavior as the melting behavior observed in DSC (Table 2). The following region in Figure 8b, at which both moduli G' and G'' are nearly stable with raising temperature, is called the rubbery plateau.[44] First, both neat polyethylene grades show an elastic behavior in the melt state because the shear storage moduli G' take higher values than loss moduli G''. Further, the height of G' depends on the number of crosslinks and entanglements.[43,45]

Shear storage modulus G' and shear loss modulus G'' for the photooxidized PE-HD 1 present a systematic decrease after UV-exposure (Figure 8c). This reduction of

TABLE 2 Compilation of crystallinity and melting peak temperature for first and second DSC heating curve for both PE-HD

	X_c (%)		$T_{p,m}$ (°C)	
H (MJ/m^2)	First heating	Second heating	First heating	Second heating
PE-HD 1				
0	70 ± 1	72 ± 2	135 ± 1	134 ± 2
460	72 ± 1	73 ± 1	135 ± 1	133 ± 1
PE-HD 2				
0	79 ± 1	82 ± 3	141 ± 1	139 ± 1
460	86 ± 1	68 ± 1	143 ± 1	134 ± 1

Abbreviations: DSC, differential scanning calorimetry; PE-HD, high-density polyethylene.

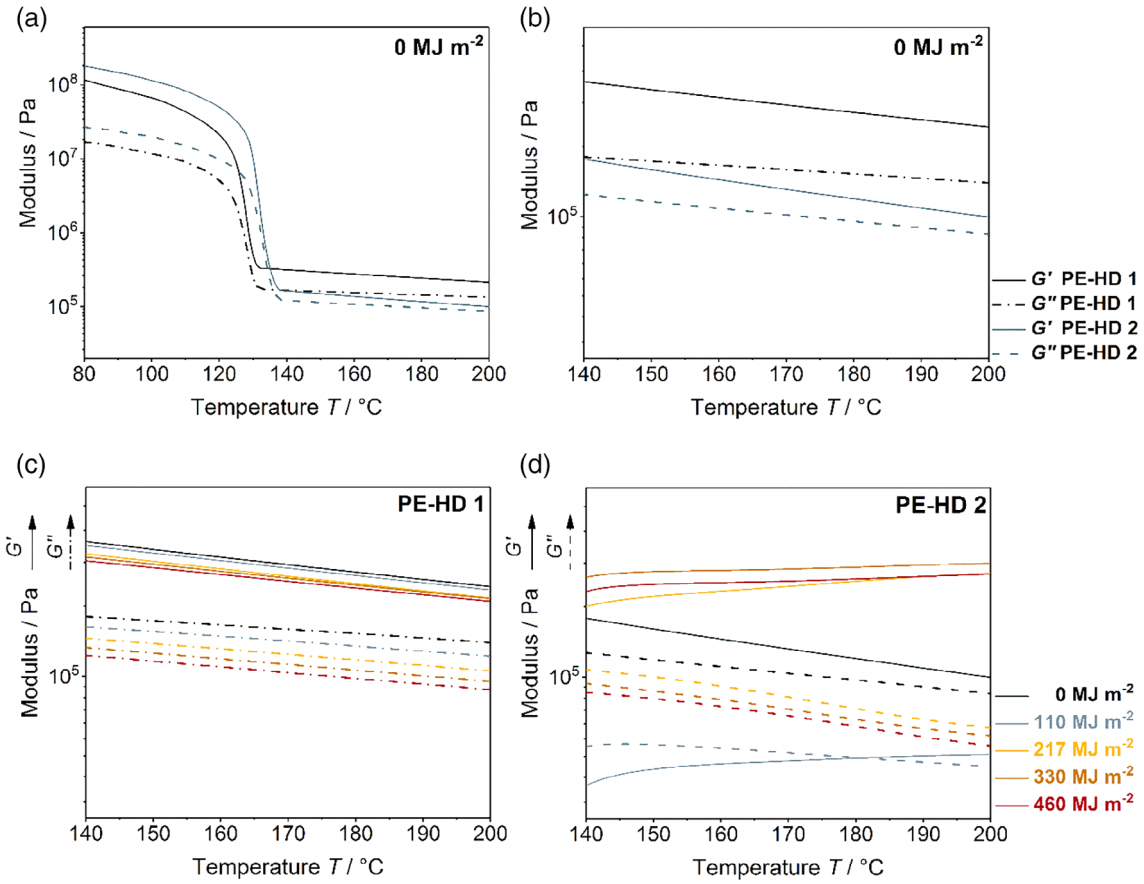

FIGURE 8 Progression of shear storage modulus G' and shear loss modulus G'' on both unexposed (0 MJ/m^2) PE-HD 1 and PE-HD 2 in the temperature range from 80 to 200°C (a), in the temperature range from 140 to 200°C (b), exposed to UV-irradiation energy H of 0, 110, 217, 330, and 460 MJ/m^2 for PE-HD 1 (c) and for PE-HD 2 (d) [Color figure can be viewed at wileyonlinelibrary.com]

both moduli G' and G'' can be attributed to a predominately UV-induced chain scission for PE-HD 1 (C—C cleavage in the main chain). The unchanged continuous decrease of G' with increasing temperature does also not indicate a significant crosslinking. It can be concluded that the still available stabilizer in PE-HD 1 (better stabilized) inhibits the oxidative chain reaction of the alky and/or alkoxy radical as detected in the lower evolution of the hydroxyl/ hydroperoxides (OH/OOH) and the carbonyl absorption region (C═O). Also, the prolonged ductile impact behavior in Charpy test (Figures 4 and 5), the still existing oxidation resistance (OIT) and the almost unchanged first melting curve in the DSC (Table 2) support this finding. The stabilizer most likely inhibits the photooxidative reaction, but shorter chain fragments are formed, leading to the lowering of the storage modulus G'.

In contrast to that, the shear storage moduli G' of the UV-irradiated PE-HD 2 samples reveal an increase of the absolute values with increasing exposure levels (217, 330, and 460 MJ/m^2). Furthermore, G' exhibits a positive temperature dependence, that is, the storage modulus increases with increasing temperature, while G'' (progressively) decreases (Figure 8d). This is in agreement with the classical theory of rubber elasticity and therefore is a strong indication of a dominating crosslinking,[45,46] as also observed in the hindered recrystallization ability as inferred from the reduced crystallinity values for the second heating in DSC. It has to be noted that since the heating rate used in DMA (3 K/min) is somewhat lower than in DSC (10 K/min), it cannot be completely excluded that the photooxidation products aldehydes and ketones (α,β-unsaturated) may undergo crosslinking when reaching the rubbery plateau during the measurement. This would result in the formation of new intermolecular bonds leading to a steady increase of the molecular weight[5] as observed by the raising storage modulus G' over the temperature (see Figure 8d).

Again, the presented data for PE-HD 2 suggest that the stabilizer is already consumed at the lowest UV-irradiation energy, as also indicated by the sudden drop of the Charpy impact strength at 38 MJ/m^2.

4 | CONCLUSIONS

In conclusion, it could be demonstrated that the instrumented Charpy impact test is a sensitive mechanical method to detect even early stages of material deterioration of high-density polyethylene induced by photooxidation. Structural changes induced by UV-irradiation in PE-HD can be easily recognized by analysis of the recorded load–deflection curves during impact test. The evaluation of the fracture constituents, crack initiation energy W_i and crack propagation energy W_p, provides additional information on the fracture behavior. This would not be possible by the conventional Charpy impact test, since it determines only an integral fracture energy. Furthermore, the detailed analysis of the resulting fracture surfaces reveals important details about the fracture process.

From the Charpy impact test it could be deduced that the progressing deterioration by UV-irradiation reduces the overall impact strength and results in increasing contributions of brittle features on the fracture surface. For one material the pronounced UV-induced embrittlement leads to an anomalous fracture with a reversed direction of crack propagation, that is, the crack initiation occurred at the hammer impact and not at the preformed notch as intended for the test.

For the investigated PE-HD materials, a completely brittle fracture is observed when the impact strength a_{cN} is reduced to at least half of its respective initial value. This is mainly due to a diminishing of the crack propagation energy W_p in the load–deflection curve to practically zero while crack initiation energy W_i and maximum impact load remain nearly constant.

The two investigated polymers presented a different resistance to UV-irradiation as revealed also by their OIT indicating a better stabilization of PE-HD 1 by antioxidants. This is clearly reflected by the instrumented Charpy impact test and the further shown methods. In case of PE-HD 1, the deterioration of the impact properties proceeds continuously with increasing UV-exposure and only a lower carbonyl-build up is observed. On the contrary, PE-HD 2 showed a distinctly lower resistance to UV-irradiation, manifested by an immediate decline of the impact strength to drastically lower values (upon 38 MJ/m^2). Also, the pronounced carbonyl evolution indicates extensive oxidation and the significantly increased crystallinity is a result of considerable UV-induced chain scission. Furthermore, the simultaneous occurrence of crosslinking is unambiguously proven by the limited recrystallization in the second heating run (DSC) and the higher storage modulus G' in the rubbery plateau (DMA), which also shows a distinct increase with increasing temperature.

ACKNOWLEDGMENTS

The authors would like to thank Oliver Schwarze and Nicolai Schmidt for sample preparation. Markus Schilling's assistance in the instrumented Charpy impact tests is kindly acknowledged. This work was supported by BAM within the project “Microbiologically influenced corrosion” (MIC) in the focus area “Material”.

CONFLICT OF INTEREST

The authors declare no conflicts of interest.

DATA AVAILABILITY STATEMENT

The raw data required to reproduce these findings cannot be shared at this time as the data also forms part of an ongoing study. The processed data required to reproduce these findings cannot be shared at this time as the data also forms part of an ongoing study.

ORCID

Maren Erdmann https://orcid.org/0000-0002-0641-5675
Ute Niebergall https://orcid.org/0000-0002-4970-7627
Volker Wachtendorf https://orcid.org/0000-0001-9549-7416
Martin Böhning https://orcid.org/0000-0001-9753-345X

REFERENCES

[1] A. J. Peacock, *In Handbook of Polyethylene: Structures, Properties, and Applications*, Vol. 1, Marcel Dekker, New York **2000**.
[2] P. Gijsman, G. Meijers, G. Vitarelli, *Polym. Degrad. Stab.* **1999**, *65*, 433.
[3] M. C. Celina, *Polym. Degrad. Stab.* **2013**, *98*, 2419.
[4] A. L. Andrady, in *In Physical Properties of Polymers Handbook*, Vol. 2 (Ed: J. E. Mark), Springer, New York **2007**; Chapter 51, p. 857.
[5] J. F. Rabek, *Photodegradation of Polymers: Physical Characteristics and Applications*, Vol. 1, Springer-Verlag, Berlin, Heidelberg **1996**.
[6] J. L. Bolland, G. Gee, *J. Chem. Soc., Faraday Trans.* **1946**, *42*, 236.
[7] B. Fayolle, E. Richaud, X. Colin, J. Verdu, *J. Mater. Sci.* **2008**, *43*, 6999.
[8] I. H. Craig, J. R. White, A. V. Shyichuk, I. Syrotynska, *Polym. Eng. Sci.* **2005**, *45*, 579.
[9] A. Quintana, M. C. Celina, *Polym. Degrad. Stab.* **2018**, *149*, 173.
[10] K. T. Gillen, R. L. Clough, *Polymer* **1992**, *33*, 4358.
[11] B. Fayolle, X. Colin, L. Audouin, J. Verdu, *Polym. Degrad. Stab.* **2007**, *92*, 231.
[12] A. F. Reano, A. Guinault, E. Richaud, B. Fayolle, *Polym. Degrad. Stab.* **2018**, *149*, 78.
[13] B. Fayolle, L. Audouin, J. Verdu, *Polym. Degrad. Stab.* **2000**, *70*, 333.
[14] L. C. Mendes, E. S. Rufino, F. O. C. de Paula, A. C. Torres Jr.., *Polym. Degrad. Stab.* **2003**, *79*, 371.

[15] A. Torikai, H. Shirakawa, S. Nagaya, K. Fueki, *J. Appl. Polym. Sci.* **1990**, *40*, 1637.
[16] L. Audouin, V. Langlois, J. Verdu, J. C. M. J. de Bruijn, *Mater. Sci.* **1994**, *29*, 569.
[17] J. Pospíšil, J. Pilař, N. C. Billingham, A. Marek, Z. Horák, S. Nešpůrek, *Polym. Degrad. Stab.* **2006**, *91*, 417.
[18] U. Niebergall, J. Bohse, B. L. Schürmann, S. Seidler, W. Grellmann, *Polym. Eng. Sci.* **1999**, *39*, 1109.
[19] V. N. Hristov, R. Lach, W. Grellmann, *Polym. Test.* **2004**, *23*, 581.
[20] N. M. Stark, L. M. Matuana, *Polym. Degrad. Stab.* **2004**, *86* (1), 1.
[21] J. Tanks, S. Sharp, D. Harris, *Polym. Test.* **2016**, *51*, 63.
[22] ISO 179-1 Plastics—Determination of Charpy impact properties—Part 1: Non-instrumented impact test, **2010**.
[23] M. Böhning, U. Niebergall, A. Adam, W. Stark, *Polym. Test.* **2014**, *34*, 17.
[24] M. Böhning, U. Niebergall, A. Adam, W. Stark, *Polym. Test.* **2014**, *40*, 133.
[25] R. A. C. Deblieck, D. J. M. van Beek, M. McCarthy, P. Mindermann, K. Remerie, B. Langer, R. Lach, W. Grellmann, *Polym. Eng. Sci.* **2017**, *57*, 13.
[26] M. Erdmann, M. Böhning, U. Niebergall, *Polym. Degrad. Stab.* **2019**, *161*, 139.
[27] ISO 293:2004 Plastics—Compression moulding of test specimens of thermoplastic materials, **2004**.
[28] M. Böhning, U. Niebergall, M. Zanotto, V. Wachtendorf, *Polym. Test.* **2016**, *50*, 315.
[29] M. Erdmann, A. Kupsch, B. R. Müller, M. P. Hentschel, U. Niebergall, M. Böhning, G. Bruno, *J. Mater. Sci.* **2019**, *54*(17), 11739.
[30] ISO 4892-3:2013 Plastics—Methods of exposure to laboratory light sources—Part 3: Fluorescent UV lamps, **2013**.
[31] DIN EN ISO 4892-1:2016-10 Plastics—Methods of exposure to laboratory light sources—Part 1: General guidance (ISO 4892-1:2016), German version EN ISO 4892-1:2016, **2016**.
[32] Atlas, https://www.atlas-mts.com/products/testingservices/natural-weathering/natural-weathering-testing-sites/north-american-sites/florida-benchmark-testing-sites (accessed: February 2018).
[33] ISO 179-2:1997 + Amd.1:2011 Plastics—Determination of Charpy impact properties—Part 2: Instrumented impact test; German version EN ISO 179-2:1999 + A1:2012179–2:1997, **2012**.
[34] W. Grellmann, S. Seidler, *In Polymer Testing*, Vol. 1, Hanser Gardner Publications, Munich **2007**.
[35] DIN EN ISO 11357-3:2018–07 Plastics—Differential scanning calorimetry (DSC)—Part 3: Determination of temperature and enthalpy of melting and crystallization (ISO 11357-3:2018), **2018**.
[36] ISO 11357-6:2018 Plastics—Differential scanning calorimetry (DSC)—Part 6: Determination of oxidation induction time (isothermal OIT) and oxidation induction temperature (dynamic OIT), **2018**.
[37] M. Hesse, H. Meier, B. Zeeh, *In Spektroskopische Methoden in der organischen Chemie*, 7th ed., Thieme, Stuttgart **2005**.
[38] M. Gardette, A. Perthue, J.-L. Gardette, T. Janecska, E. Földes, B. Pukánszky, S. Therias, *Polym. Degrad. Stab.* **2013**, *98*, 2383.
[39] M. S. Rabello, J. R. White, *Polymer* **1997**, *38*, 6379.
[40] S. A. Jabarin, E. A. J. Lofgren, *Appl. Polym. Sci.* **1994**, *53*, 411.
[41] K. T. Gillen, M. Celina, R. L. Clough, *Radiat. Phys. Chem.* **1999**, *56*, 429.
[42] J. V. Gulmine, P. R. Janissek, H. M. Heise, L. Akcelrud, *Polym. Degrad. Stab.* **2003**, *79*, 385.
[43] A. Kömmling, K. von der Ehe, D. Wolff, M. Jaunich, *Radiat. Phys. Chem.* **2018**, *142*, 29.
[44] L. H. Sperling, *In Introduction to Physical Polymer Science*, 4th ed., Wiley, New York **2006**.
[45] K. P. Menard, *In Dynamic Mechanical Analysis: A Practical Introduction*, 2nd ed., CRC Press, Boca Raton, London, New York **2008**.
[46] G. Rehage, *Pure Appl. Chem.* **1974**, *39*, 161.

SUPPORTING INFORMATION

Additional supporting information may be found online in the Supporting Information section at the end of this article.

How to cite this article: Erdmann M, Niebergall U, Wachtendorf V, Böhning M. Evaluation of UV-induced embrittlement of PE-HD by Charpy impact test. *J Appl Polym Sci*. 2020;137: e49069. https://doi.org/10.1002/app.49069